Enhanced reversible solid-state photoswitching of a cationic dithienylethene assembled with a polyoxometalate unit

P. Bolle,[a] C. Menet,[a] M. Puget,[a] H. Serier-Brault,[a] S. Katao,[c] V. Guerchais,[b] F. Boucher,[a] T. Kawai,[c*] J. Boixel,[b*] and R. Dessapt[a*]

[a.] *Université de Nantes, CNRS, Institut des Matériaux Jean Rouxel, IMN, F-44000 Nantes, France. E-mail: remi.dessapt@cnrs-imn.fr*

[b.] *Univ Rennes, CNRS, ISCR – UMR6226, F-35000, Rennes, France. E-mail: julien.boixel@univ-rennes1.fr*

[c.] *Graduate School of Materials Science, Nara Institute of Science and Technology, 8916-5 Takayama, Ikoma, Nara 630-0192, Japan. E-mail: tkawai@ms.naist.jp*
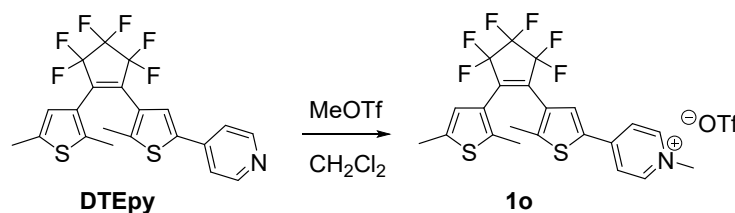
Electronic Supporting Information

Experimental

Chemicals and reagents:

All chemicals and reagents were purchased from major chemical suppliers and used as received except $(NBu_4)_4[\alpha-Mo_8O_{26}]^{S1}$ which has been synthesized according to the reported procedure.

Synthesis of 1-OTf

DTEpy   MeOTf / CH₂Cl₂   **1o**

The triflate salt of **1o** (**1-OTf**) was isolated as a yellow-green powder by methylation of the **DTEpy** derivative with methyl trifluoromethanesulfonate (950 mg, 85 %). **DTEpy** was prepared following a reported multi-step procedure.[S2] Single crystals of **1-OTf** were obtained according to the following procedure: **1-OTf** (0.041 g, 0.066 mmol) was dissolved in dichloromethane (2 mL). The resulting yellow/green solution was stirred at 30 °C for 10 minutes, filtered and kept at ambiant temperature. Beige single-crystals of **1-OTf** were isolated from the solution after one day. Elemental Analysis. Calcd for $C_{23}H_{18}NO_3S_3F_9$: C, 44.26; H, 2.88; N, 2.24; S, 15.39. Found: C, 42.29; H, 2.94; N, 2.08; S, 14.98. ESI-HRMS. Calcd for $C_{22}H_{18}NS_2F_6$, z=1, m/z: 474.07794. Found: 474.0784 (1 ppm). ^1H NMR (400 MHz; CD₂Cl₂): δ 8.66 (d, 2H), 8.00 (d, 2H), 7.86 (s, 1H), 6.74 (s, 1H), 4.40 (s, 3H), 2.43 (s, 3H), 2.05 (s, 3H), 1.88 (s, 3H). ^{19}F NMR (376 MHz; MeOD): δ -80.12 (3F, s), -111.25 (2F, m), -112.09 (2F,

m), -133.59 (2F, quint). ^{13}C NMR (100 MHz; MeOD): δ 151.2, 149.4, 146.7, 140.3, 136.5, 132.5, 129.2, 125.6, 125.5, 123.4, 54.8, 47.9, 15.0, 14.9, 14.4. FT-IR (KBr cm^{-1}): 3126 (w), 3077 (sh), 3051 (m), 2929 (w), 2863 (w), 1639 (s), 1553 (m), 1516 (m), 1496 (w), 1477 (w), 1452 (m), 1427 (w), 1335 (m), 1303 (sh), 1271 (vs), 1229 (m), 1192 (m), 1173 (w), 1138 (s), 1113 (s); 1092 (w), 1053 (m), 1032 (s), 986 (m), 962 (sh), 899 (w), 886 (w), 854 (m), 827 (w), 758 (w), 740 (w), 734 (w), 636 (s), 577 (w), 565 (sh), 538 (w), 518 (m), 489 (m), 440 (w).

Synthesis of (1)$_4$[Mo$_8$O$_{26}$]·4DMF (1-Mo$_8$)

(NBu$_4$)$_4$[α-Mo$_8$O$_{26}$] (0.065 g, 0.030 mmol) was dissolved in acetonitrile (3 mL). The colourless solution (solution 1) was stirred for a few minutes at room temperature. In addition, a second solution (solution 2) is obtained by dissolving **1-OTf** (0.075 g, 0.120 mmol) in acetonitrile (2 mL) at room temperature. Solution 2 was added dropwise to solution 1 under vigorous stirring leading to the precipitation of a beige solid. The mixture was stirred at 40 °C for two hours, kept at room temperature, and then filtered. The powder was washed with few milliliters of acetonitrile, then ethanol, and dried in air. Then the powder was dissolved in DMF (2 mL). The resulting yellow/green solution was stirred at 50 °C for one hour, filtered and kept at ambient temperature. Beige single-crystals of **1-Mo$_8$** were isolated from the solution after few days. Yield in Mo: 40%. Elemental Analysis Calcd for C$_{100}$H$_{100}$N$_8$O$_{30}$Mo$_8$S$_8$F$_{24}$: C, 35.59; H, 2.96; N, 3.32. Found: C, 35.35; H, 2.88; N, 3.05. FT-IR (KBr cm^{-1}): DMF 1672 (vs), 1661 (vs), 1454 (sh), 1441 (m), 1406 (w), 1387 (m) ; υ1o: 3128 (w), 3089 (sh), 3051 (m), 1643 (vs), 1551 (m), 1516 (m), 1477 (m), 1337 (s), 1304 (sh), 1275 (vs), 1232 (w), 1190 (s), 1136 (s), 1113 (s); 1051 (s), 989 (s) ; υMo=O, υMo-O-Mo 947 (vs), 908 (vs), 847 (w), 835 (s), 804 (sh), 731 (m), 714 (s), 660 (s), 630 (sh), 577 (w), 559 (w), 523 (m), 478 (m), 451 (w).

Physical Measurements:

- Elemental analyses of the solids were performed by the "Service de microanalyses ICSN CNRS, in Gif sur Yvette (France) and the CRMPO (Centre de Mesures Physiques de l'Ouest) in Rennes.
- NMR spectra were recorded on Bruker, AV 330 and AV 400 spectrometers. ^{1}H, and ^{13}C chemical shifts are reported in parts per million (ppm), determined by reference to residual solvent signals. ^{19}F chemical shifts, also in ppm, are reported without internal reference.
- High Resolution Mass Spectrum was recorded on a Bruker maXis+ (ESI-QTOF).
- FT-IR spectra were recorded in the 4000-400 cm^{-1} range on a BRUKER Vertex equipped with a computer control using the OPUS software.
- Intensity data collections were carried out with Bruker-Nonius Kappa CCD diffractometer using Mo K-L$_{2,3}$ radiation (λ = 0.71073 Å) with a graphite monochromator a Bruker Nonius X8 APEX 2 diffractometer equipped with a CCD bidimensional detector using Mo Kα monochromatized radiation (λ = 0.71073 Å) for **1-OTf** (CCDC 2012275), with a Bruker-Nonius X8 APEX 2 diffractometer equipped with a CCD bidimensional detector using Mo Kα monochroma-tized radiation (λ = 0.71073 Å) for **1-Mo$_8$** (CCDC 2060278), and with a Rigaku R-AXIS RAPID diffractometer using multi-layer mirror monochromated Mo-Kα radiation for **1-Mo$_8$** after irradiation with 365 nm light (CCDC 2012299). The absorption corrections were based on multiple and symmetry-equivalent reflections in the data set using the SADABS program[S3] based on the method of Blessing.[S4] The structure were solved by direct methods and refined by full-matrix least-squares

using the SHELX-TL package.[S5] The hydrogen atoms were theoretically located on the basis of the conformation of the supporting atoms. Obtained structures were visualized and plotted with the Diamond program. These data can be obtained free of charge via www.ccdc.cam.ac.uk/conts/ retrieving.html (or from the Cambridge Crystallographic Data Centre, 12 Union Road, Cambridge CB21EZ, U.K.; fax (44) 1223-336-033; email deposit@ccdc.cam.ac.uk).

- Diffuse reflectance spectra were collected at room temperature on a finely ground sample with a Perkin-Elmer Lambda 1050 spectrometer equipped with a 60 mm diameter integrating sphere coated with Spectralon®, a highly reflecting fluoropolymer. Diffuse reflectance was measured from 250 to 1000 nm with a 2 nm step using Halon powder (from Varian) as reference (100% reflectance). $((CH_3CH_2)_2NH_2)_2(NH_4)_2[Mo_8O_{26}]$ which was used as an optical reference of the β-$[Mo_8O_{26}]^{4-}$ unit was synthesized as previously described.[S6] The reflectance data were treated by a Kubelka-Munk transformation[S7] to better determine the absorption thresholds. The photocoloration and fading kinetics were quantified by monitoring the temporal evolution of the photogenerated absorption $Abs^{\lambda max}(t)$ defined as $Abs^{\lambda max}(t) = -\log(R^{\lambda max}(t)/R^{\lambda max}(0))$, where $R^{\lambda max}(t)$ and $R^{\lambda max}(0)$ are the reflectivities at the time t and at $t = 0$, respectively. For the coloration kinetics, the samples were irradiated with a Fisher Bioblock labosi UV lamp ($\lambda_{ex} = 365$ nm, P = 6W) at a distance of 50 mm. $Abs^{\lambda max}(t)$ *vs.* t plots have been fitted according to a biexponential rate law $Abs^{\lambda max}(t) = (A_1 + A_2) - A_1\exp(-k^c_1 t) - A_2\exp(-k^c_2 t)$, with k^c_1 and k^c_2 the extracted coloration rate constants. For the bleaching processes, the samples were first irradiated under 365 nm-UV excitation until the photoinduced absorptions reach saturation. Then, the compounds were put under Thorlabs LED Array light sources (630 nm - 2.4 W/cm^2) at a distance of 100 mm. The bleaching kinetics were determined at room temperature by monitoring the temporal decays of $Abs^{\lambda max}(t)$ of samples once irradiated. $Abs^{\lambda max}(t)$ *vs.* t plots have been fitted according to a monoexponential rate law $Abs^{\lambda max}(t) = (A_0 - A_1) + A_1\exp(-k^f t)$, with k^f the extracted fading rate constant.

Electronic Structure Calculations:

- Ground-state electronic structures were obtained within the DFT formalism using the Perdew-Burke-Ernzerhof parametrization of the generalized gradient approximation (PBE-GGA).[S8] Calculations have been carried out with the ab initio total energy and molecular dynamics program VASP (Vienna ab initio simulation package).[S9] Projector augmented-wave (PAW) pseudopotentials were used.[S10] Atomic positions were optimized by minimizing the residual Hellmann-Feynman forces on the atoms. The self-consistency on electronic density was obtained with a 550-eV plane-wave energy cutoff and a (2×1×1) Monkhorst-Pack k-point mesh [2 k points in the irreducible part of the Brillouin zone (IBZ)]. Forces on atoms were minimized down to 0.02 eV/Å for the structural relaxations.

- The frequency-dependent dielectric functions were obtained by using the linear optic routines implemented in VASP, this frequency dependence being evaluated up to 40 eV. Thus, Kohn-Sham wave functions have been evaluated for many additional empty bands (2500 bands above the Fermi level). The reaction energy pathways between **1o** and **1c** conformers was evaluated within the transition state theory formalism using the Nudged Elastic Band method as implemented in the VTST tools.

Figure S1. ^{1}H NMR (300 MHz; CD$_2$Cl$_2$) spectra of **1-OTf**, (a) before and (b) after UV irradiation (5 min at 365 nm.
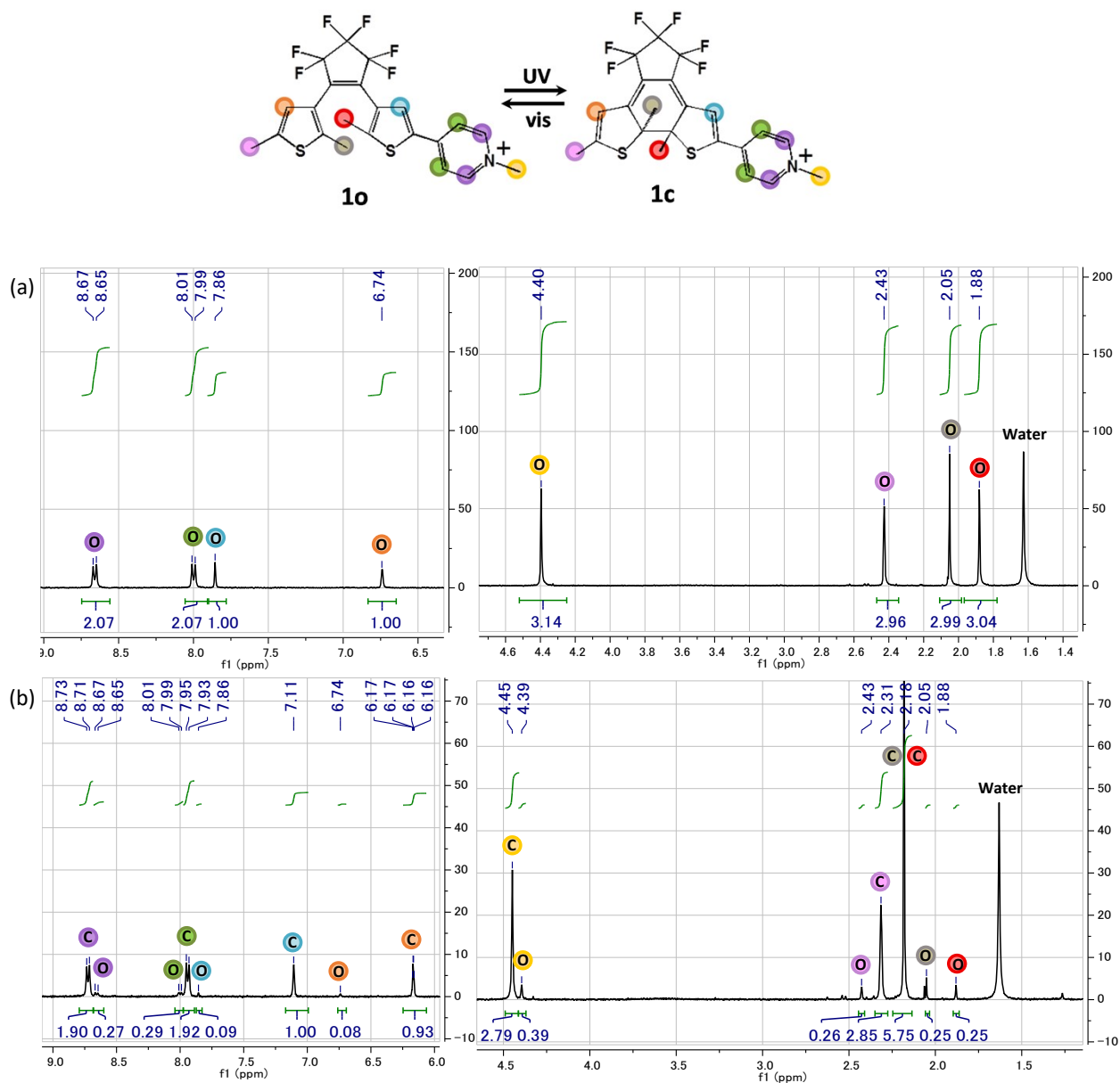
All the peaks were attributed to the hydrogens of **1o** or **1c**, respectively noted with the symbols (o) and (c). The average percentage of photoconversion is 90 % and was determined from the values found for all hydrogen atoms.
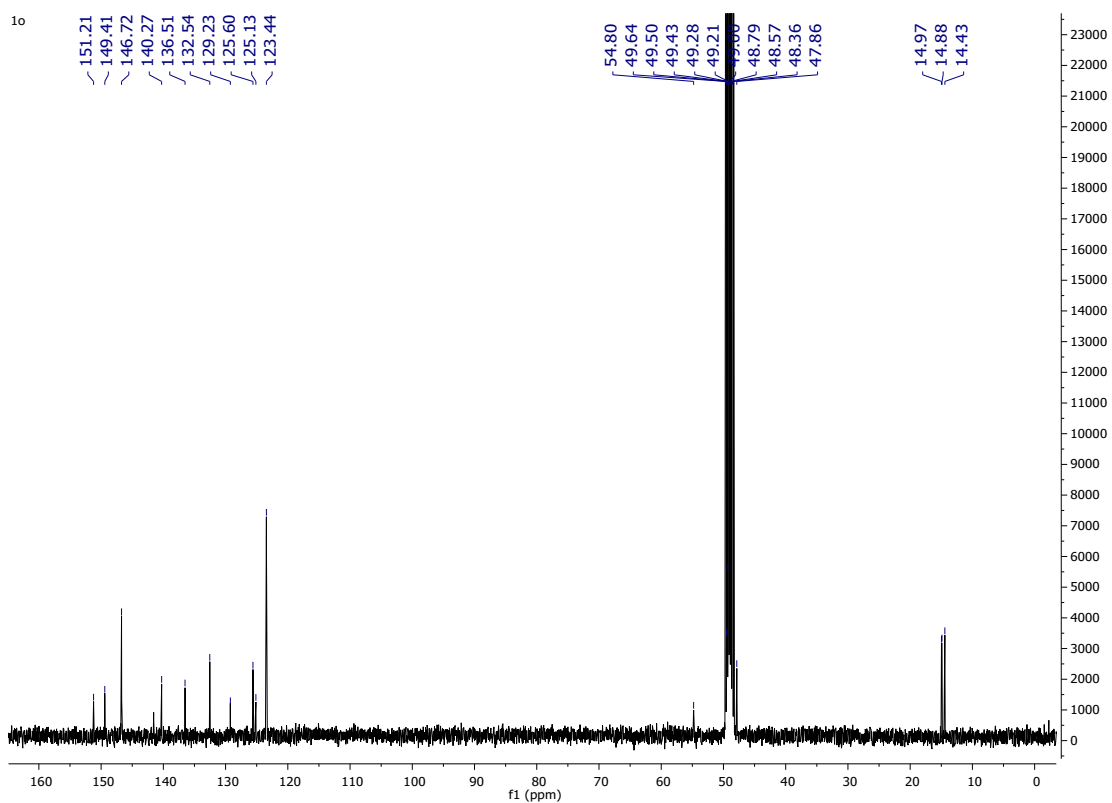
- **1o (δ ppm):**

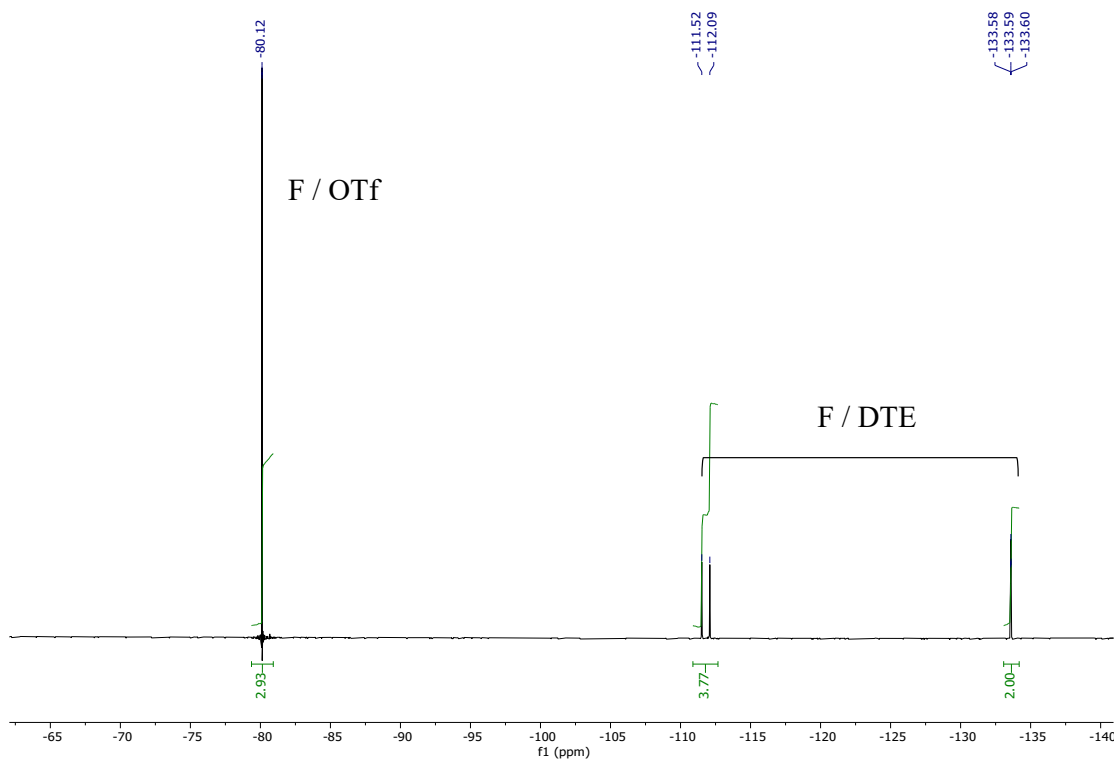8.66 (d, 2H), 8.00 (d, 2H), 7.86 (s, 1H), 6.74 (s, 1H), 4.39 (s, 3H), 2.43 (s, 3H), 2.05 (s, 3H), 1.88 (s, 3H).

- **1c (δ ppm):**

8.72 (d, 2H), 7.94 (d, 2H), 7.11 (s, 1H), 6.17 (s, 1H), 4.45 (s, 3H), 2.31 (s, 3H), 2.18 (s, 6H).

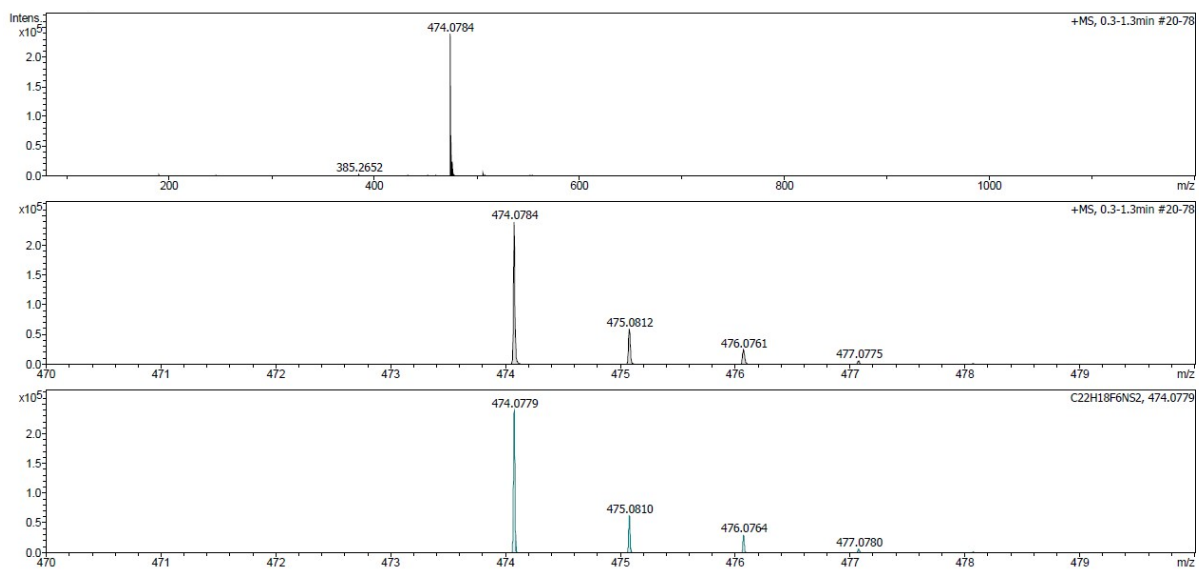**Figure S2.** ^{13}C NMR (100 MHz; MeOD) spectrum of **1-OTf**.

**Figure S3.** ^{19}F NMR (376 MHz; MeOD) spectrum of **1-OTf**.

5

Figure S4. ESI-HRMS spectra of **1o**.

Figure S5. Ball-and-stick representations of the crystal structure of **1-OTf**. (a) Structure of the **1o** cation. The C···C distance between the reactive carbons is indicated as a red dotted line. (b) Assembly of the **1o** molecules into supramolecular ribbons running along the *b*-axis. (c) Stacking of the **1o** molecules and the triflate anions. (grey sphere: carbon; purple sphere: fluoride; yellow sphere: sulfide; green sphere: nitrogen; orange sphere: oxygen). H-atoms are omitted for clarity.
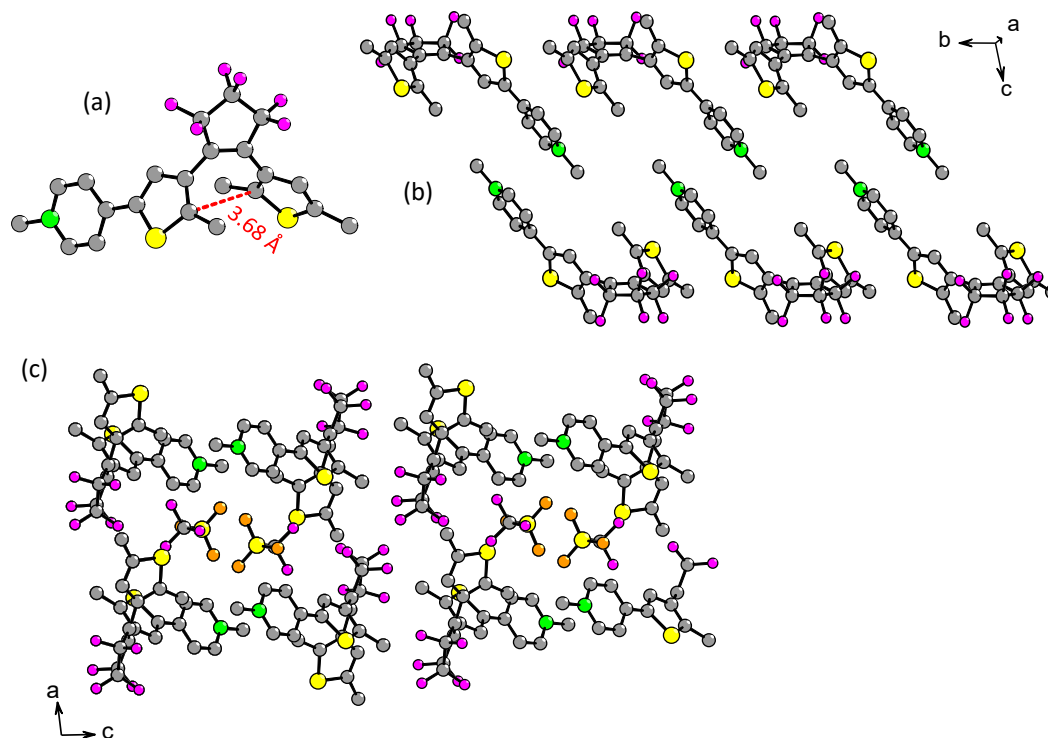

Figure S6. Room-temperature UV-vis absorption spectra of **1-OTf** in CH_2Cl_2 (5.3 .10^{-5} mol. L^{-1}), after 0 sec (black line) and 20 secs (blue line) upon irradiation at 365 nm.
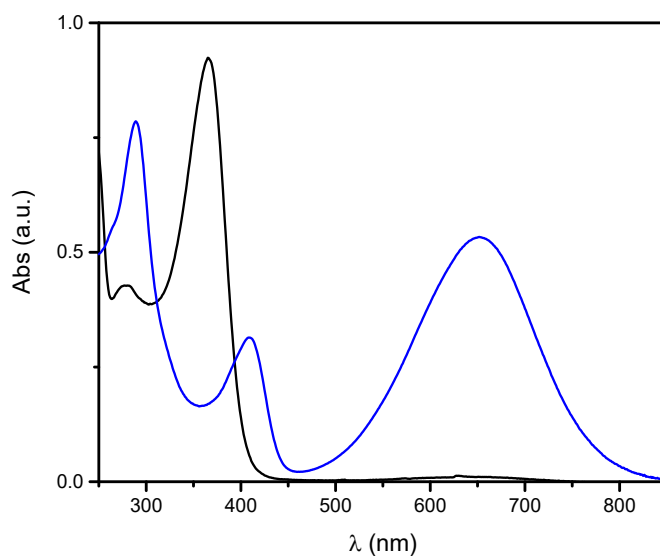
Figure S7. Determination of the molar extinction coefficient (ε) of the absorption band at $\lambda_{max} = 366$ nm of the open-ring **1o** form in CH_2Cl_2 solution.
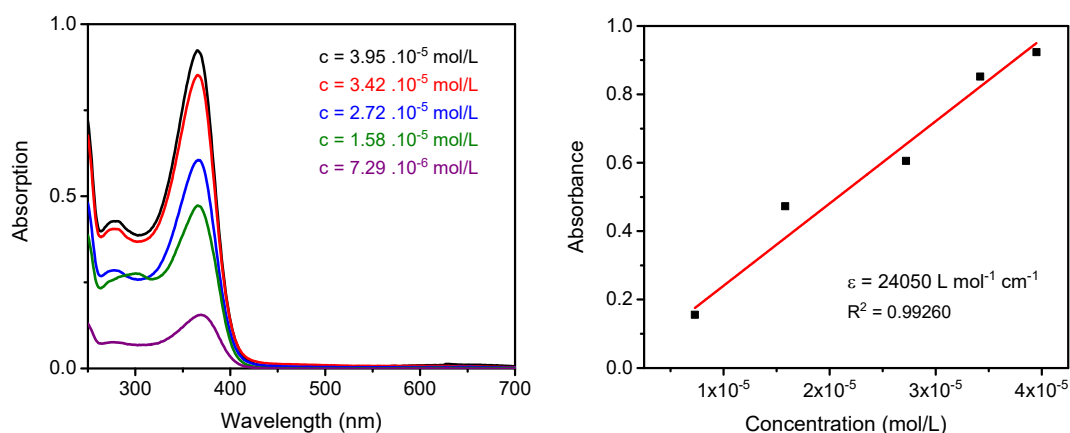
Figure S8. Determination of the molar extinction coefficient (ε) of the absorption band at $\lambda_{max} = 409$ nm (top) and 653 nm (bottom) of the closed-ring **1c** form in CH_2Cl_2 solution. Each spectrum was monitored after irradiation upon 365 nm for 180 secs.
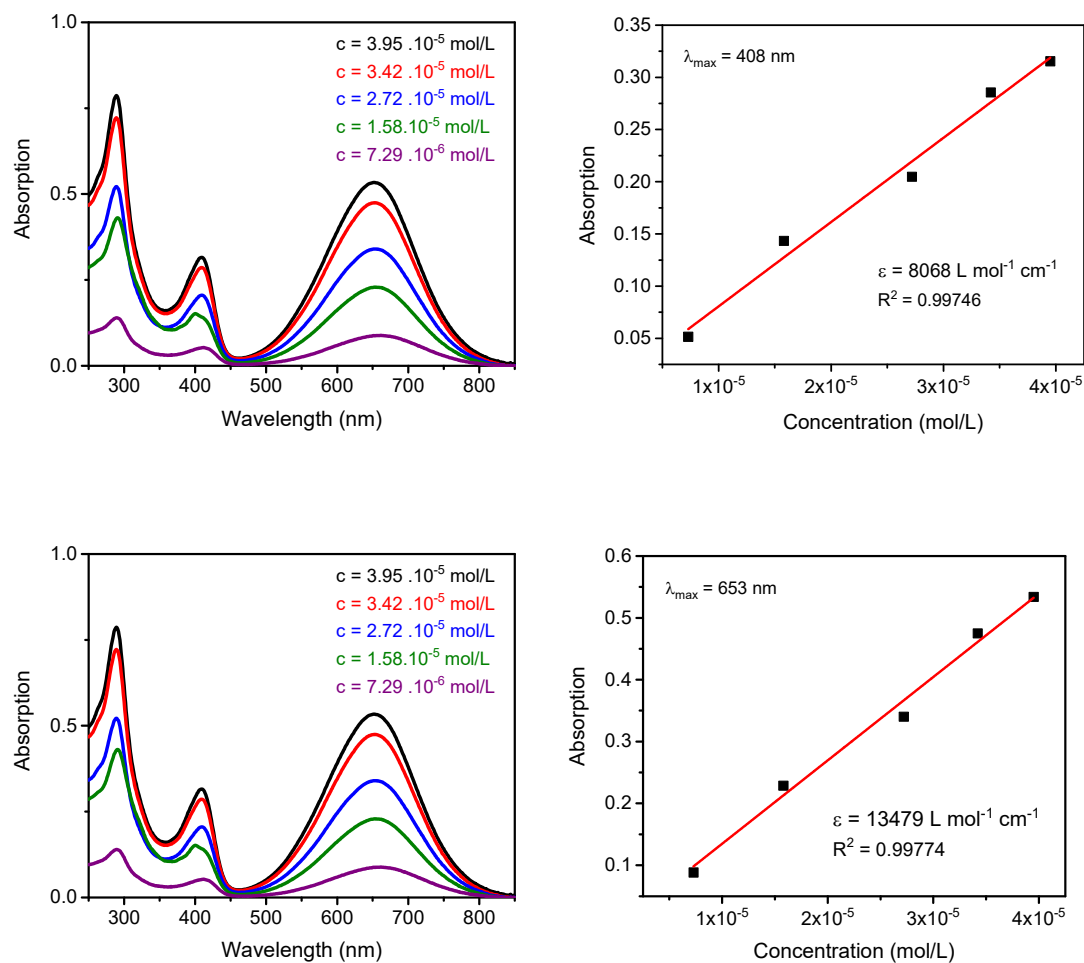
Figure S9. Comparison of the FT-IR spectra of (a) **1-OTf** and (b) **1-Mo$_8$**.
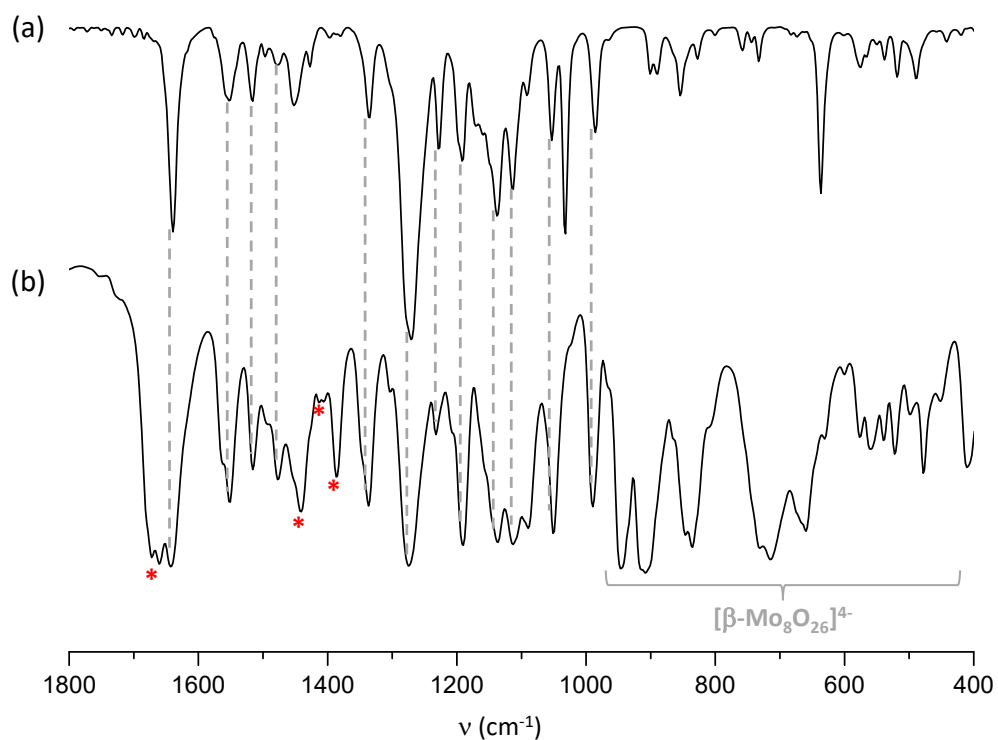

In the spectrum of **1-Mo$_8$,** the strong absorption bands in the range 1000-400 cm^{-1} were attributed to the Mo=O and Mo-O-Mo vibration modes of the β-[Mo$_8$O$_{26}$]$^{4-}$ anion. The absorption bands in the range of 1650-1000 cm^{-1} are mainly assigned to the vibration modes of the **1o** molecule, while the absorption bands indicated by an asterisk are assigned to the vibration modes of the crystallized DMF molecules.

Figure S10. Representation of the supramolecular assembly of POMs with head-to-tail dimers of 1o_1 cations in **1-Mo$_8$**.
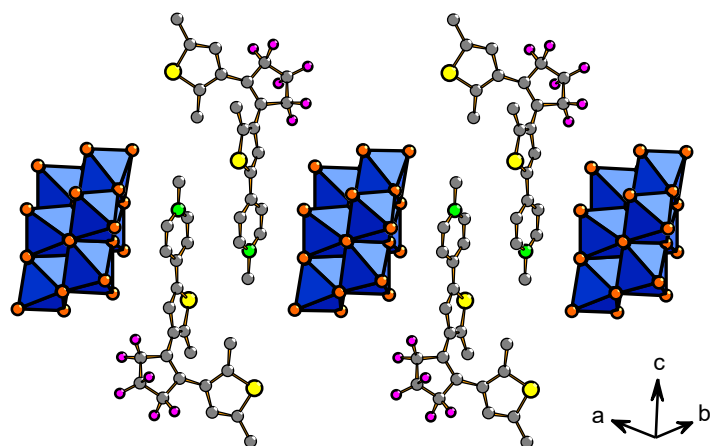

Figure S11. Kubelka-Munk transformed reflectivity spectra of **1-Mo$_8$** (red line), **1-OTf** (black line) and ((CH$_3$CH$_2$)$_2$NH$_2$)$_2$(NH$_4$)$_2$[β-Mo$_8$O$_{26}$] (blue line).
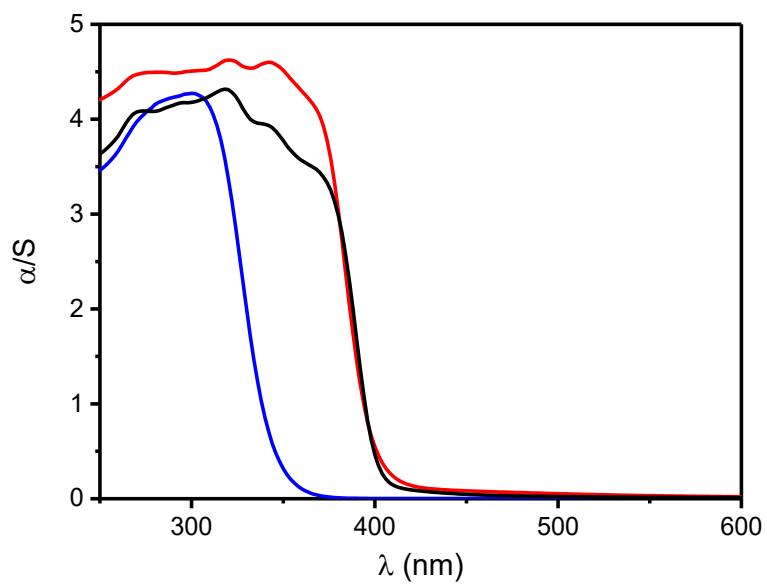
Figure S12. Photographs of the photochromic properties of **1-OTf** upon 0, 2 and 5 min of 365 nm-UV irradiation at room temperature, and evolution of its absorption spectrum after 0, 0.166, 0.5, 1, 2, 3, 5, 10 and 20 min of UV irradiation (λ_{ex} = 365 nm).
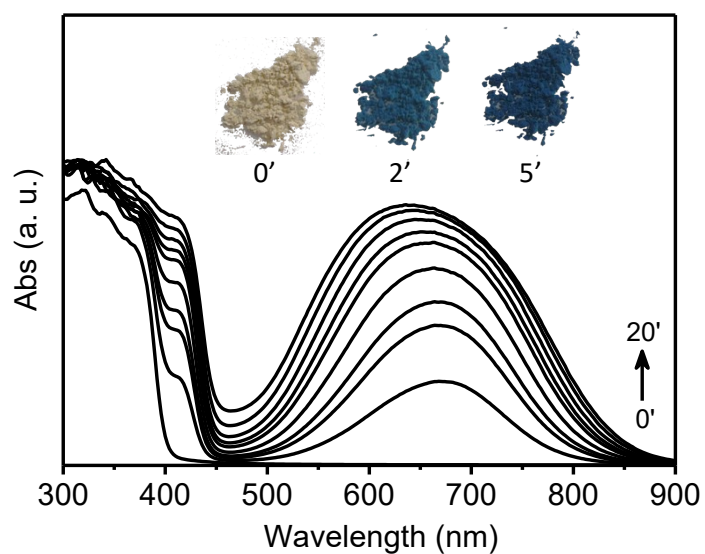

Figure S13. Temporal evolution of the photogenerated absorption of (a) **1-OTf** and (b) **1-Mo$_8$** after 0, 0.166, 0.333, 0.5, 1, 2, 3, 4, 5, 10, 20 and 30 min of 365 nm-UV irradiation.
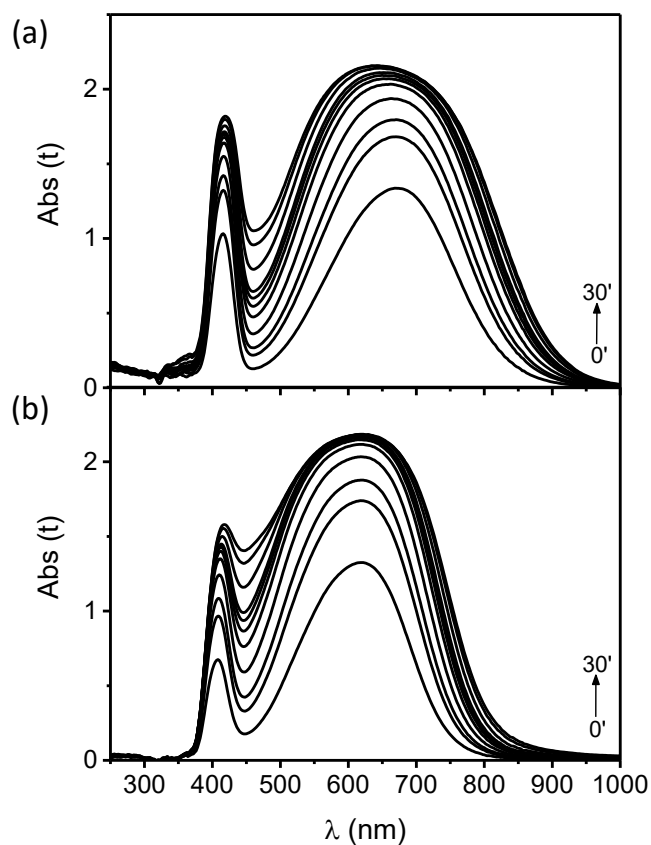
Figure S14. Temporal evolutions of the absorbance at λ_{max} = 670 nm at room temperature for **1-OTf** under 365 nm-UV irradiation (□), in the dark during the thermal fading (□) and under visible light (λ_{exc} = 630 nm) (□). The solid lines show the fits of the $Abs^{670}(t)$ *vs. t* plots according to rate laws $Abs^{670}(t)$ = $(A_1 + A_2) - A_1\exp(-k^c_1 t) - A_2\exp(-k^c_2 t)$ for the photocoloration process, and $Abs^{670}(t) = (A_0 - A_1) + A_1\exp(-k^f_1 t)$ for the fading process under visible light. The black dashed line shows the absorbance value just before switching off UV irradiation. The percentage of absorbance lost after 180 mins under visible light is also indicated.
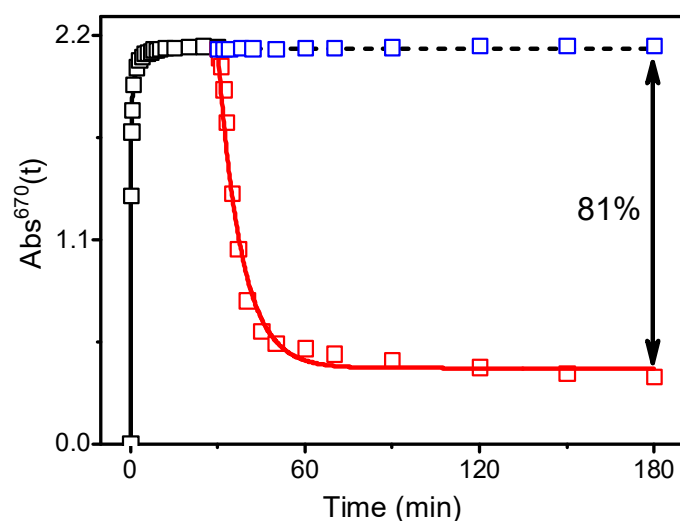
Figure S15. Evolution of the absorbance monitored at 618 nm for **1-Mo$_8$** during successive coloration/bleach cycles (*n*) at room temperature. In each cycle, the sample was irradiated for 10 secs with UV light (365 nm) and then for 4 min with red light (630 nm). The solid red line corresponds to the linear fit of $Abs^{618}(n)$ *vs. n* according to the empirical linear relationship: $Abs^{618}(n)$ = - 0.002n + 1.296, which predicts that the color-change effect should disappear at the end of about 650 cycles.
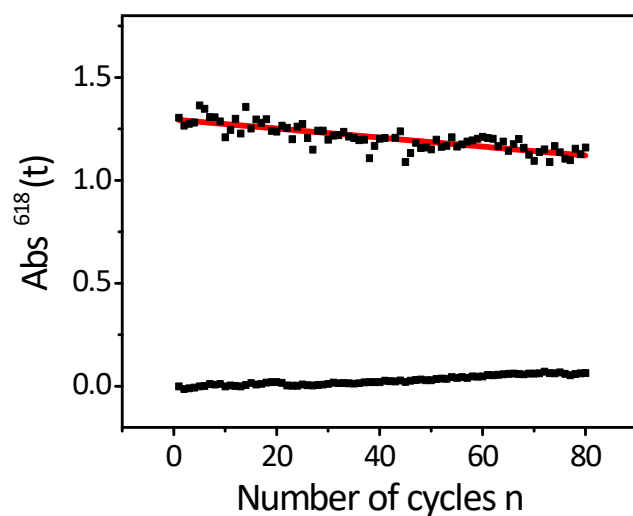
Figure S16. (a) Polyhedral and ball-and-stick representation of the crystal packing in **1-Mo$_8$** after irradiation with 365 nm UV light. The disordered structure shows a mixture of open-ring **1o** (blue atoms) and closed-ring **1c** (red atoms) isomers in a 1o/1c ratio of 72:28 for 1o/c_1 and of 73:27 for 1o/c_2, estimated from the occupancy factors. (b) Superimposed structures of the **1o** (blue atoms) and **1c** (red atoms) cations. No change in position has been observed for the atoms of the pyridinium group of 1o/c_2. (blue octahedra = MoO$_6$, blue, red and grey sphere: carbon, yellow sphere: sulfur, orange sphere: oxygen, green sphere: nitrogen). H and F atoms are omitted for clarity.
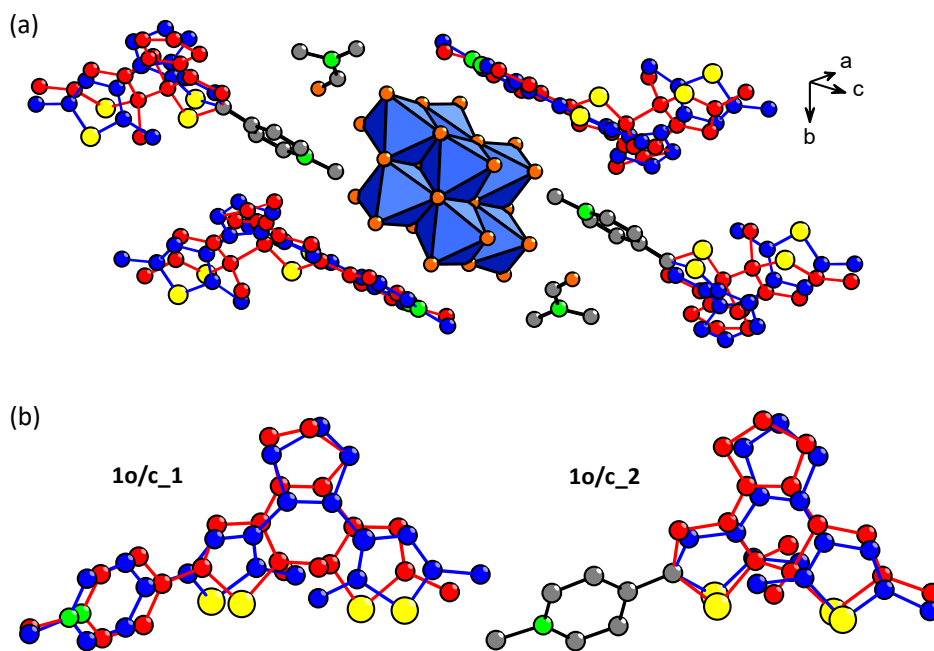
Figure S17. Minimum energy path of transition between the open-ring **1o** (left) and the closed-ring **1c** (right) conformers of **1-Mo$_8$**.
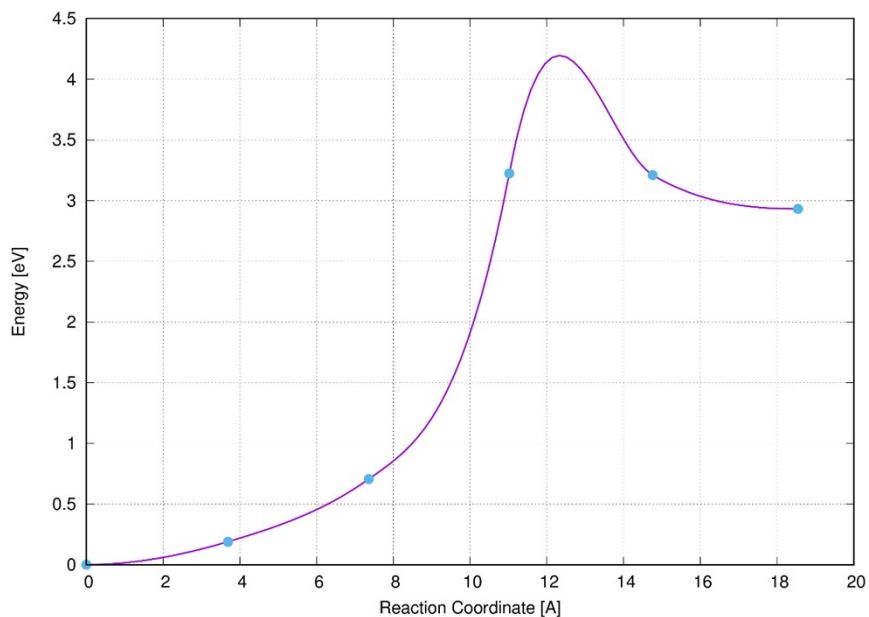
Total energy of the closed-ring **1c** conformer of **1-Mo$_8$** (right) is found roughly 3 eV/unit cell above total energy of the open-ring **1o** conformer of **1-Mo$_8$** (left). The closed-ring **1c** conformer is found to be a metastable configuration which stay stable at least up to 300K. No thermal conversion was overserved using ab initio molecular dynamics. Energy barrier difference between the cyclization (4.2 eV from **1o** to **1c)** and the cycloreversion (1.3 eV from **1c** to **1o**) is coherent with the difference in the wavelengths needed for the photoexcitation of those processes (365 nm and 650 nm, respectively).

Figure S18. Superimposition of the two calculated structures of **1-Mo₈** containing the open-ring **1o** (blue atoms) and closed-ring **1c** (red atoms) conformers (left), compared to the experimental crystal structure after irradiation with 365 nm UV light (right). (blue octahedra = MoO₆, blue, red and grey sphere: carbon and fluorine, yellow sphere: sulfur, orange sphere: oxygen, green sphere: nitrogen). F atoms of the experimental structure are not displayed. H atoms are omitted for clarity.
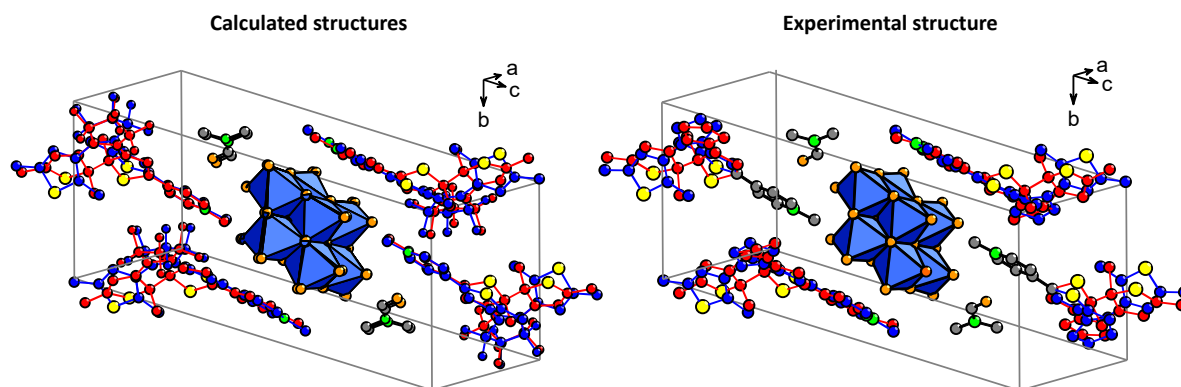

Figure S19. Left: Superimposed positioning of POM units and DMF molecules in the two calculated structures of **1-Mo₈** containing the **1o** (DMF molecules with blue C-atoms) and **1c** (DMF molecules with red C-atoms). Right: Thermal ellipsoid drawings (50%) of the POM unit and DMF molecules in the experimental crystal structure after irradiation with 365 nm UV light. (blue octahedra = MoO₆, blue, red and grey sphere: carbon, orange sphere: oxygen, green sphere: nitrogen). H atoms are omitted for clarity.
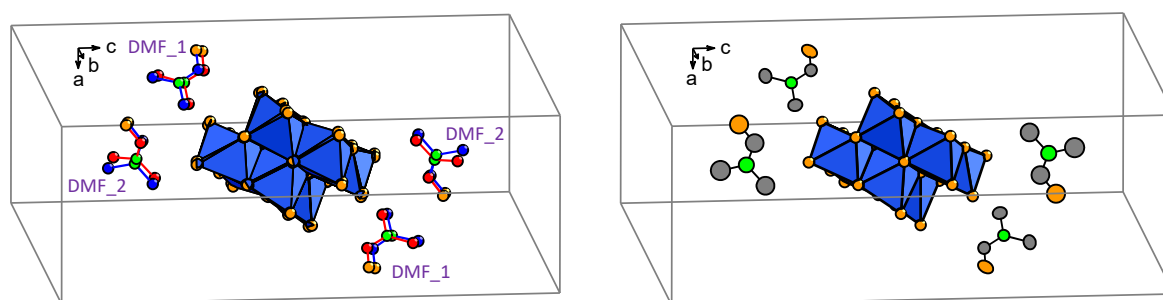
In the experimental crystal structure, the thermal ellipsoids around the C, N and O atoms of the DMF molecules indicate disorder, but it was not possible to model this in a satisfactory way. The superimposition of the two calculated structures well confirm motions of the DMF molecules in the crystal lattice before and after UV-light irradiation, which is more marked for DMF_2 than for DMF_1, in perfect line with the experimental atomic displacement parameters.

Figure S20. Top: Comparison of the molecular geometries and bond lengths of the **1c** closed-ring isomers of the DTE cations in the calculated (left) and experimental (right) structures of **1-Mo₈**. Bottom: molecular geometry and bond lengths of the closed-ring isomer of the bis(2,5-dimethyl-3-thienyl)perfluorocyclopentene whom structure of the closed-ring isomer was solved by X-ray crystallography.[S11] (grey sphere: carbon; magenta sphere: fluorine, yellow sphere: sulfur, green sphere: nitrogen). H atoms of the calculated closed-ring isomers are omitted for clarity.

bis(2,5-dimethyl-3-thienyl)perfluorocyclopentene
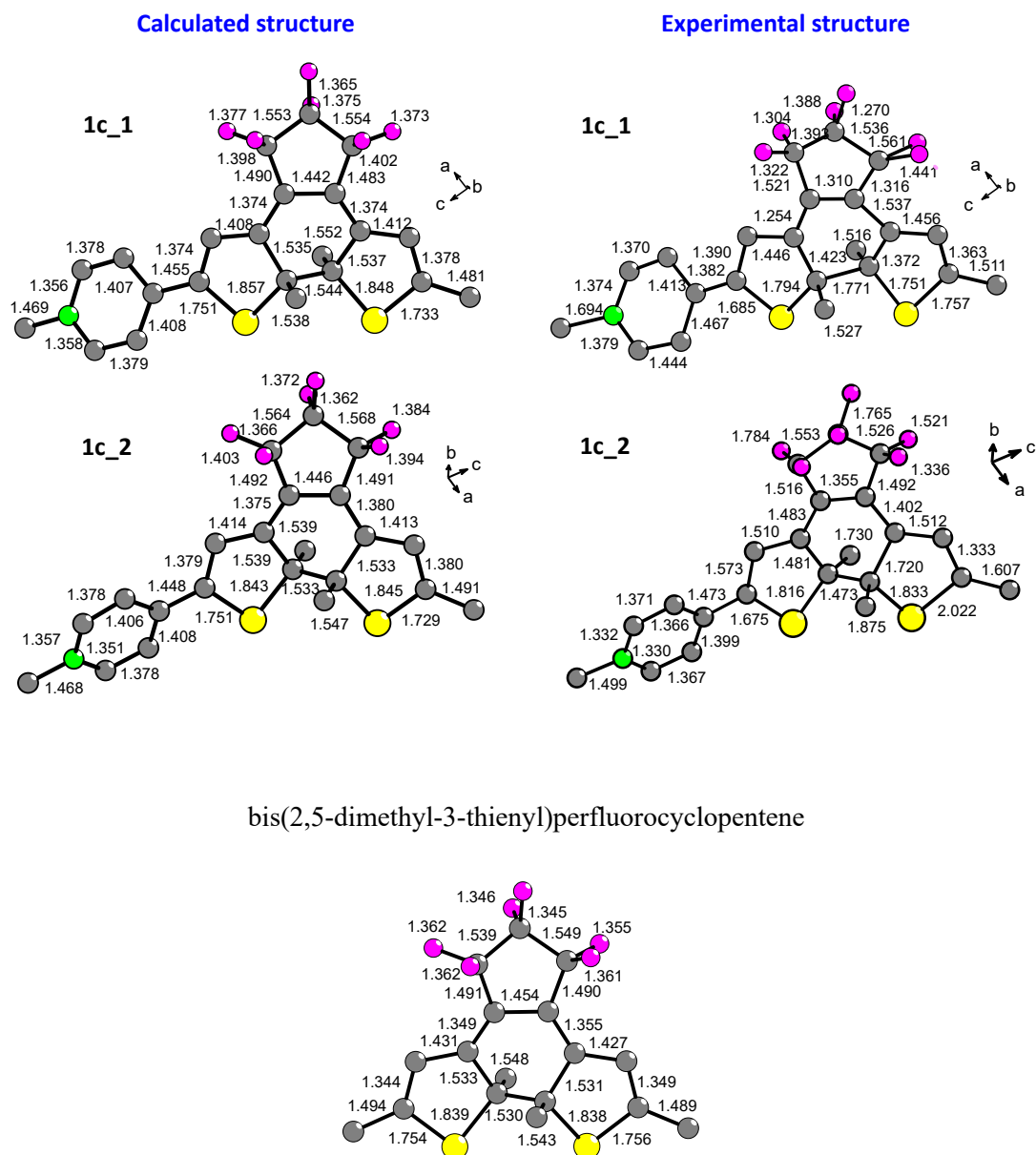
In the calculated structure of **1-Mo₈**, the bond lengths in the **1c** isomers are in perfect agreement with those of the reported bis(2,5-dimethyl-3-thienyl)perfluorocyclopentene in its closed-ring form. In particular, double and single bond alternation around the fused ring of 1c_1 and 1c_2 in **1-Mo₈** are well observed. Moreover, in both calculated **1c** molecules, the bond lengths of the two inner C-S bonds implying the reactive carbon atoms of the thiophene groups (1.843-1.857 Å) are longer than the two outer C-S bonds (1.729-1.751 Å). This is well expected for closed-ring DTEs since S-C(sp³) single bond would be longer than S-C(sp²) single bond.

16

Figure S21. Total and partial density of states of the two calculated structures of **1-Mo$_8$** containing the open-ring **1o** (top) and closed-ring **1c** (bottom) conformers.

Open ring: DOS, partial DOS, and atomic proportion

Closed ring: DOS, partial DOS, and atomic proportion
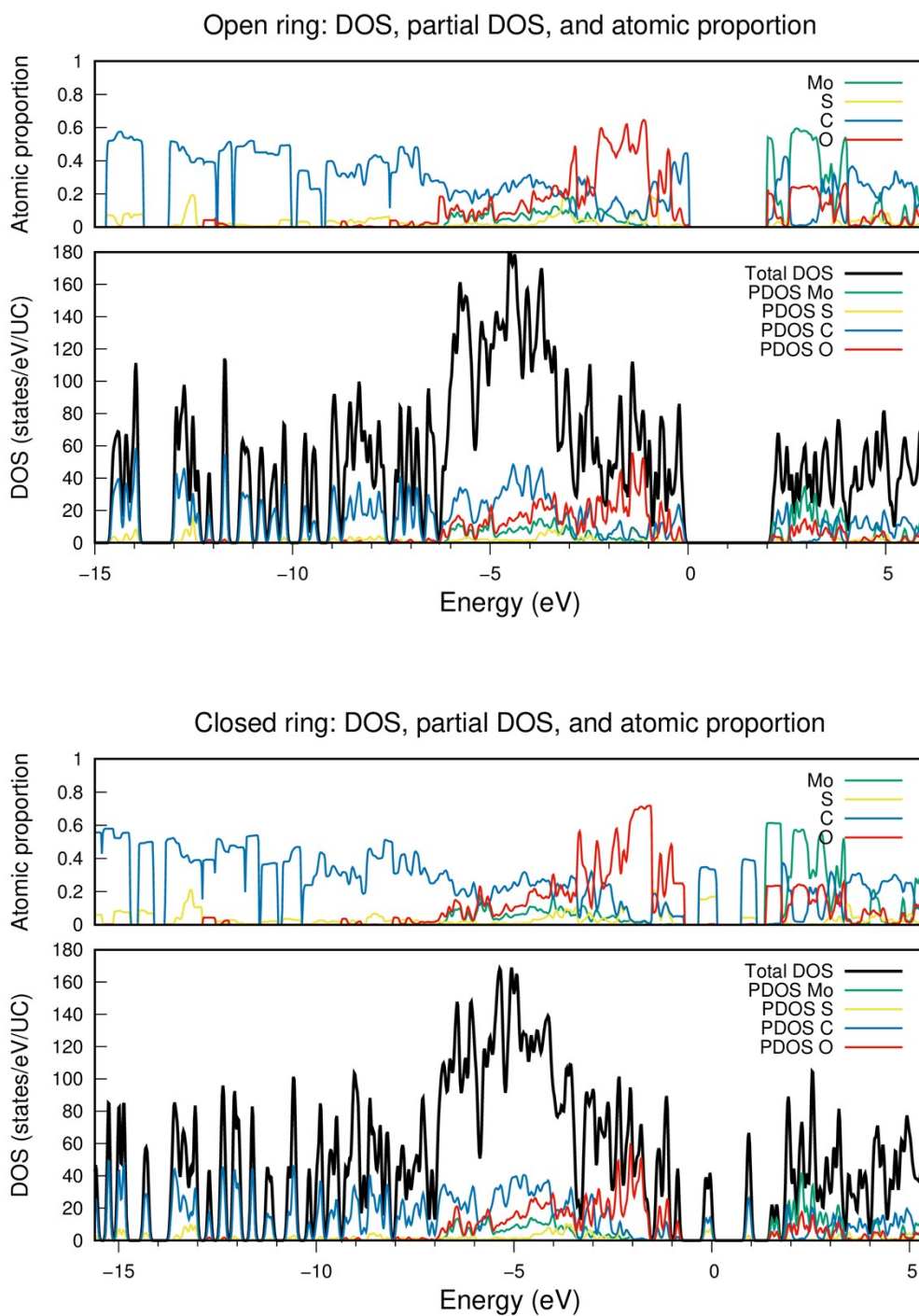
In the calculated structure of **1-Mo$_8$,** the top of the valence band in the open ring conformer comes from carbon bands. Those bands move into the gap in the close ring conformer with the appearance of bonding and antibonding C-C bands. Energy references are taken at Fermi levels.

Table S1. Crystal data and structure refinement for **1-OTf** and **1-Mo₈**.

Compound	1-OTf	1-Mo$_8$	1-Mo$_8$ after irradiation
Chemical composition	$F_9S_3O_3NC_{23}H_{18}$	$Mo_8F_{24}S_8O_{30}N_8C_{100}H_{100}$	$Mo_8F_{24}S_8O_{30}N_8C_{100}H_{100}$
Formula weight	623.56	3373.87	3373.87
Temperature (K)	293 K	291 K	123 K
Crystal system	Triclinic	Triclinic	Triclinic
Space group	P-1 (2)	P-1 (2)	P-1 (2)
a/Å	8.6007(17)	10.2777(2)	10.2122
b/ Å	9.5704(19)	11.4846(2)	11.28910
c/ Å	16.715(3)	26.8984(5)	26.68000
α/°	102.92(3)	88.001(1)	86.57
β/°	92.57(3)	86.893(1)	86.8060
γ/°	105.59(3)	84.001(1)	85.0870
Volume/ Å^3	1283.6(5)	3151.57(10)	3055.09
Z	2	1	1
ρ_{calc} (g/cm^3)	1.568	1.778	1.794
μ/mm^{-1}	0.380	1.010	1.039
F(000)	597.0	1676	1604
Crystal size/mm^3	0.3 × 0.2 × 0.1	0.4 × 0.2 × 0.1	0.12 × 0.11 × 0.02
Radiation	Mo Kα (λ = 0.71073)	Mo Kα (λ = 0.71073)	Mo Kα (λ = 0.71073)
2Θ range for data collection/°	4.56 to 70.00	3.91 to 60.22	3.62 to 54.97
Index ranges	-12 ≤ h ≤ 13 -15 ≤ k ≤ 15 -26 ≤ l ≤ 26	-14 ≤ h ≤ 14 -13 ≤ k ≤ 16 -37 ≤ l ≤ 37	-12 ≤ h ≤ 13 -14 ≤ k ≤ 14 -34 ≤ l ≤ 34
Reflections collected	62704	54622	50688
Independent reflections	11270 [R_{int} = 0.0587]	18488 [R_{int} = 0.0328]	14004 [R_{int} = 0.0655]
Data/parameters	11270/356	18488/814	14004/739
Goodness-of-fit on F^2	1.017	0.933	1.049
Final R indexes [I>=2σ (I)]	R_1 = 0.0676, wR_2 = 0.1529	R_1 = 0.0416, wR_2 = 0.1080	R_1 = 0.0812, wR_2 = 0.2193
Final R indexes [all data]	R_1 = 0.1648, wR_2 = 0.1962	R_1 = 0.0761, wR_2 = 0.1350	R_1 = 0.1032, wR_2 = 0.2397
Largest diff. peak/hole/ eÅ^{-3}	0.63/-0.48	1.715/-0.706	1.64/-1.90
CCDC number	2012275	2060278	2012299

Table S2. Photochromic kinetic parameters at room temperature of **1-OTf** and **1-Mo$_8$**.

Photocoloration process under UV-light irradiation (λ_{ex} = 365 nm)

Compound	A$_1$[a]	A$_2$[a]	k$^c_1$ ×10^3 (s^{-1})[b]	k$^c_2$ ×10^3 (s^{-1})[b]	t$^c_{1/2}$ (min)[c]	R^{2} [d]
1-OTf	0.408	1.720	10.9 ± 0.9	138.1 ± 4.3	0.12	0.9995
1-Mo$_8$	0.391	1.790	15.0 ± 1.0	123.4 ± 2.5	0.12	0.9998

Fading process under visible-light irradiation (λ_{ex} = 630 nm)

Compound	A$_0$[a]	A$_1$[a]	k$^f_1$ ×10^3 (s^{-1})[b]	t$^f_{1/2}$ (min)[c]	R^{2} [d]
1-OTf	2.128	1.720	2.06 ± 0.2	5.6	0.9878
1-Mo$_8$	2.181	2.118	3.22 ± 0.3	3.5	0.9822

The coloration kinetics of **1-OTf** and **1-Mo$_8$** has been quantified by monitoring the photogenerated absorption band at respectively λ = 670 nm and λ = 618 nm (Abs(t)) as a function of UV irradiation time t. [a]The Abs(t) vs t plots were fitted as Abs(t) = (A$_1$+A$_2$) - A$_1$exp($-$k^c_1t) - A$_2$exp($-$k^c_2t) for the coloration process, and as Abs(t) = (A$_0$$-A_1$) + A$_1$exp($-k^f_1$t) for the fading process under visible-light irradiation. [b]Coloration (k^c) and fading (k^f) rate constants. [c]For the coloration process, the half-life time $t^c_{1/2}$ is defined as the UV irradiation time required for Abs(t) to reach half of its maximum value. For the fading process under visible-light irradiation, $t^f_{1/2}$ is respectively defined as the irradiation time required for Abs(0) to reach the A$_0$ $-$ A$_1$/2 value. [d]Regression coefficient for the Abs(t) vs t plots.

References

S1   W. G. Klemperer, *Inorganic Syntheses*, John Wiley & Sons, Ltd, 1990, 74–85.

S2   M. Liu, G. Liu and S. Q. Cui, *Appl. Mech. Mater.*, 2012, **164**, 239–242.

S3   G. M. Sheldrick, *SADABS Program Scaling Correct. Area Detect. Data Univ. Gött. Gött. Ger.*, 1997.

S4   R. H. Blessing, *Acta Crystallogr. Sect. A*, 1995, **51**, 33–38.

S5   G. M. Sheldrick, *SHELX-TL Softw. Package CrystalStruc-Ture Determ. Siemens Anal. X-Ray Instrum. Divi-Sionversion 503 Bruker AXS Inc Madison WI.*

S6   K. Hakouk, O. Oms, A. Dolbecq, H. El Moll, J. Marrot, M. Evain, F. Molton, C. Duboc, P. Deniard, S. Jobic, P. Mialane and R. Dessapt, *Inorg. Chem.*, 2013, **52**, 555–557.

S7   P. Kubelka and F. Munk, *Z. Techn. Physik*, 1931, **12**, 593–601.

S8   J. P. Perdew, K. Burke and M. Ernzerhof, *Phys. Rev. Lett.*, 1996, **77**, 3865–3868.

S9   G. Kresse and J. Furthmüller, *Phys. Rev. B*, 1996, **54**, 11169–11186.

S10   G. Kresse and D. Joubert, *Phys. Rev. B*, 1999, **59**, 1758–1775.

S11   T. Yamada, S. Kobatake, K. Muto and M. Irie, *J. Am. Chem. Soc.*, 2000, **122**, 1589–1592.